Journal Pre-proofs

Natural Sponge-like Wood-Derived Aerogel for Solar-Assisted Adsorption and Recovery of High-viscous Crude Oil

Weixiang Chao, Shaobin Wang, Yudong Li, Guoliang Cao, Yusen Zhao, Xiaohan Sun, Chengyu Wang, Shih-Hsin Ho

PII: S1385-8947(20)31993-8
DOI: https://doi.org/10.1016/j.cej.2020.125865
Reference: CEJ 125865

To appear in: *Chemical Engineering Journal*

Received Date: 3 May 2020
Revised Date: 7 June 2020
Accepted Date: 9 June 2020

Please cite this article as: W. Chao, S. Wang, Y. Li, G. Cao, Y. Zhao, X. Sun, C. Wang, S-H. Ho, Natural Sponge-like Wood-Derived Aerogel for Solar-Assisted Adsorption and Recovery of High-viscous Crude Oil, *Chemical Engineering Journal* (2020), doi: https://doi.org/10.1016/j.cej.2020.125865

Natural Sponge-like Wood-Derived Aerogel for Solar-Assisted Adsorption and Recovery of High-viscous Crude Oil

Weixiang Chao [a], *Shaobin Wang* [c], *Yudong Li* [a], *Guoliang Cao* [b], *Yusen Zhao* [a], *Xiaohan Sun* [a], *Chengyu Wang* [a*], *Shih-Hsin Ho* [b*]

[a] Key Laboratory of Bio-Based Material Science and Technology of Ministry of Education, Material Science and Engineering College, Northeast Forestry University, Harbin, 150040, P. R. China

[b] State Key Laboratory of Urban Water Resources and Environment, School of Environment, Harbin Institute of Technology, Harbin, 150040, P. R. China

[c] School of Chemical Engineering and Advanced Materials, The University of Adelaide, Adelaide, SA 5005, Australia

*Corresponding Author

*Email: wangcy@nefu.edu.cn

*Email: stephen6949@hit.edu.cn; stephen6949@msn.com

Abstract: An efficient collection and recovery of high-viscous crude-oil from oil spillage through an environmental-friendly way is extremely important for water remediation. Herein, a new material of thermally-reduced graphene-oxide coating and decoration of hydrophobic-layer over a compressible wood-sponge was proposed as an adsorbent. Owing to the preferable photothermal conversion, an in-situ solar-assisted thermogenesis process could increase the temperature to 88 °C within 100 s under 1 sun illumination and decrease the viscosity of crude-oil for easy adsorption. The fabricated adsorbent exhibited great performances in separation and adsorption (7.28 g/g - 0.801 g/cm^3) of oil-spill; with fully active-collection of 50 mL crude-oil within 20 min. Numerical modeling was also employed to gain an in-depth understanding of the adsorption and regeneration processes. The temperature gradient and structural dots subjected to compression stress for both photothermal induced adsorption and compressible recovery of crude oil were investigated as the dominant factors. The adsorbent also exhibited satisfactory adsorption and separation capacities for common light oils and heavy oils. Moreover, the adsorbent could be employed for feasible adsorption in semi-open seawater-environment under light, showing potential for practical treatment of offshore oil-spillage. This work designed a potential route to overcome the dilemma of crude-oil adsorption, due to its inherent high-viscosity, through in-situ photothermal thermogenesis using environment-friendly materials derived from natural wood. The knowledge obtained from this work would help in developing novel adsorbents with applied and ecological merits and further understanding of the related mechanisms.

Keywords: Compressible wood adsorbent, Solar-thermal conversion, High-viscous oil adsorption, Numerical modeling calculation, In-situ thermogenesis

1. Introduction

Oil-spills have often caused severe damage to marine ecology with long-term effects [1-3]. The high-viscosity of crude-oil and its complicated recovery from oil-containing adsorbents limits the practical methods to effectively manage the crude oil spillage in most circumstances. Thus, it is crucial to have efficient approaches for separation of oil/water mixtures to mitigate environmental disasters [4-7]. Oil/water separation materials (OWSM) usually possess both hydrophobic and oleophilic properties, which can potentially clean up oil spills [8-11]. However, efficient and economic strategies for regeneration of crude oil from adsorbents are still relatively limited, which is another pivotal issue that needs to be addressed. Moreover, the detailed process and feasible mechanism of adsorption of high-viscous crude oil is beyond understanding, which actually restricts the design and application of efficient adsorbents.

Recent reports indicate that OWSM have superior separation efficiency and self-adaptive ability in various environmental conditions [12-19]. Among the numerous OWSM, porous materials with three-dimensional (3D) framework, have received considerable attention owing to their high specific surface areas with excellent adsorptivities [12, 20-23]. Synthetic sponges such as polyurethane [24] and melamine [25-28], silicone sponge [29, 30], and carbon-based porous aerogels [31-35]

have been commonly adopted to effectively separate oil/water mixtures. However, these materials suffered from many issues, such as complex and costly fabrication processes, poor environmental compatibilities, and poor mechanical strengths [12]. Thus, it is vital to develop novel adsorbents, such as OWSM frameworks with both, environmental safety and cost advantages. Wood is a renewable resource with hierarchical structure, consisting of a cellulose framework and structural support of hemicellulose and lignin [36, 37]. This characteristic structure makes it easy to convert it into porous adsorbents by treatments involving selective removal along with retention of cellulose alignments to display certain elasticity [12, 38]. This feature provides sponge-like structures, and allows for simple mechanical squeezing to recover the materials.

Crude oil has high viscosity, which heavily limits the separation efficiency. Luckily, the viscosity of crude oil decreases with increase in temperature [4, 39]. Thus, an in-situ thermogenesis within an OWSM system should accelerate the separation efficiency. Graphene, a typical two-dimensional (2D) material with a honeycomb-like sp^2 carbon lattice [40-42], can be used in a solar-to-thermal heating unit as graphene can effectively capture photons in its lattice and subsequently convert solar energy to thermal energy via lattice vibrations [43-47]. Moreover, graphene is a hydrophobic/oleophilic material with low surface oxygen and micro-nano structure [13, 15, 48-50]. Thus, graphene can be exploited as an in-situ heater to decrease the viscosity of oil. More importantly, graphene can be easily coated on the surface of an adsorbent framework with superior hydrophobic/oleophilic properties, which can

minimize the problems associated with fabrication to meet the real demands in a better way.

Herein, the aim is to solve the problems of adsorption of crude oil, due to its inherent high-viscosity and clean-up the spillage with more environment-friendly materials. This study describes the design and fabrication of a compressible biomass adsorbent based on natural wood. further decorated in-situ with reduced graphene oxide for photothermal conversion thermogenesis to lower the viscosity of crude oil for better fluidity and treatability. Hydrophobic coatings with overlayers also promoted the selective adsorption of oil phase and protected the failure of adsorbent due to immersion in water. To better understand the possible mechanism of adsorption and compressible regeneration process, numerical modeling was conducted. The temperature gradient and structural dots subjected to compression stress were investigated as the dominant factors. The knowledge obtained from this work could be useful in assessing the potential applications of using wood-based oil adsorption materials and in better understanding the corresponding mechanisms.

2. Experimental section

2.1 Materials

Balsa wood bulks were used in this work. The dimensions of the sample were 15×15×10 (mm) and the cutting direction was vertical to the growth direction of the tree. Sodium hydroxide (NaOH, ≥ 96%) and anhydrous sodium sulfite (Na_2SO_3, ≥97%) were supplied by Tianjin Dongli District Tianda Chemical Reagent Factory (China). Graphite powder (325 mesh, ≥ 99%) and octadecyltrichlorosilane (OTS)

were purchased from Aladdin (Shanghai, China). Sulfuric acid (H_2SO_4, 98%), hydrochloric acid (HCl, 36.5%) and potassium permanganate ($KMnO_4$) were purchased from Sino-pharm Chemical Reagent Co., Ltd. (Beijing, China). Ethyl alcohol (99.7%) and n-hexane (≥ 99%) were purchased from Tianjin Kemiou Chemical Reagent Co., Ltd. (Tianjin, China). Cetyl trimethyl ammonium bromide (CTAB) (99%), sodium dodecyl benzene sulfonate (SDBS) (98%), polyethylene glycol 200 (PEG 200) (99%) as surfactants were purchased from Macklin (Shanghai, China). Deionized (DI) water was prepared in the laboratory. All the chemicals were used as received without any purification.

2.2 Preparation of the wood sponge

A highly compressible wood sponge was fabricated by selective removal of lignin and hemicellulose via a two-step chemical treatment. Specifically, the wood bulks were immersed in an aqueous solution containing NaOH (2.5 mol/L) and Na_2SO_3 (0.4 mol/L), and boiled for 12 h. The delignified samples were then rinsed in triplicate with DI water to remove any traces of chemicals. Following this, the delignified wood bulks were treated with 8 wt% NaOH solution at 80 °C for 8 h to remove the hemicelluloses. The treated samples were washed with ethyl alcohol and cold DI water. Then, the wood sponge was obtained after freeze drying.

2.3 Preparation of reduced graphene oxide (GO) coated wood sponges

A GO was obtained by a modified Hummers' method [51, 52]. For the coating of reduced graphene oxide, the obtained wood sponge was initially immersed in GO dispersion and successively vacuum-dried for 10 h at room temperature. The

immersed wood sponge was then freeze dried. Then, the sample was taken in a drying dish, sealed under vacuum and dried at 100 °C for 6 h to obtain wood sponge, with an in-situ reduced graphene coating. Thereafter, a layer of transparent OTS was deposited by simple dip-coating in n-hexane to maintain its hydrophobicity and light-thermal conversion ability.

2.4 Characterizations

The morphologies and components of the samples were characterized via scanning electron microscopy (SEM) with an energy dispersive X-ray spectroscopic detector (EDX) and high-resolution transmission electron microscopy (HRTEM) for structure observation. X-ray photoelectron spectroscopy (XPS) and Fourier transform infrared spectroscopy (FT-IR) were employed to investigate the chemical composition. X-ray diffraction meter (XRD) and Raman spectroscopy were used for crystal detection. N_2 adsorption–desorption measurement according to the Brunauer–Emmett–Teller (BET) method was applied to detect porosity and pore diameter distribution. Thermogravimetric analysis (TGA) was used to determine the thermal stability, and contact angle (CA) was determined to provide information about water/oil wettability. Thermal constant analysis (TCA) was conducted for thermal conductivity both in the cross and longitudinal sections. A viscometer was used to measure the viscosity changes as a function of temperature. Measurements for viscosity of crude oil at various temperature, maximum adsorption capacity of various oils, in-situ water/crude oil wettability analysis of OWSM surface at room temperature and high temperature (80 °C) and illustration for leakage situations of

OWSM with fully adsorbed crude oil were specifically demonstrated in the supplementary information. Further information about the equipment and the testing conditions are provided in the Supplementary Information.

3. Results and discussion

3.1 Structure and properties of samples

The prepared samples were labeled as follows: PW for pristine wood, DW for delignified wood, WS for wood sponge with only cellulose framework, GO-WS for graphene oxide coated WS, rGO-WS for in-situ thermally treated GO-WS, and OTS-rGO-WS for octadecyltrichlorosilane (OTS) treated rGO-WS.

As **Figure 1a-c** illustrated, OTS-rGO-WS could be easily prepared by removal of lignin and hemicellulose, coating with GO, and subsequently decoration with OTS. Removal of lignin and hemicellulose resulted in a sponge-like compressible structure, consisting of multiple channels and pores. This permitted the adsorption of low-viscosity crude oil by capillary-force under solar illumination (**Figure 1d**). Compressible properties enabled simple recovery of adsorbed crude oil by mechanical compression as shown in **Figure 1e**. Thus, the wood-based adsorbent could achieve efficient adsorption of high-viscosity crude oil under solar illumination and recovery.

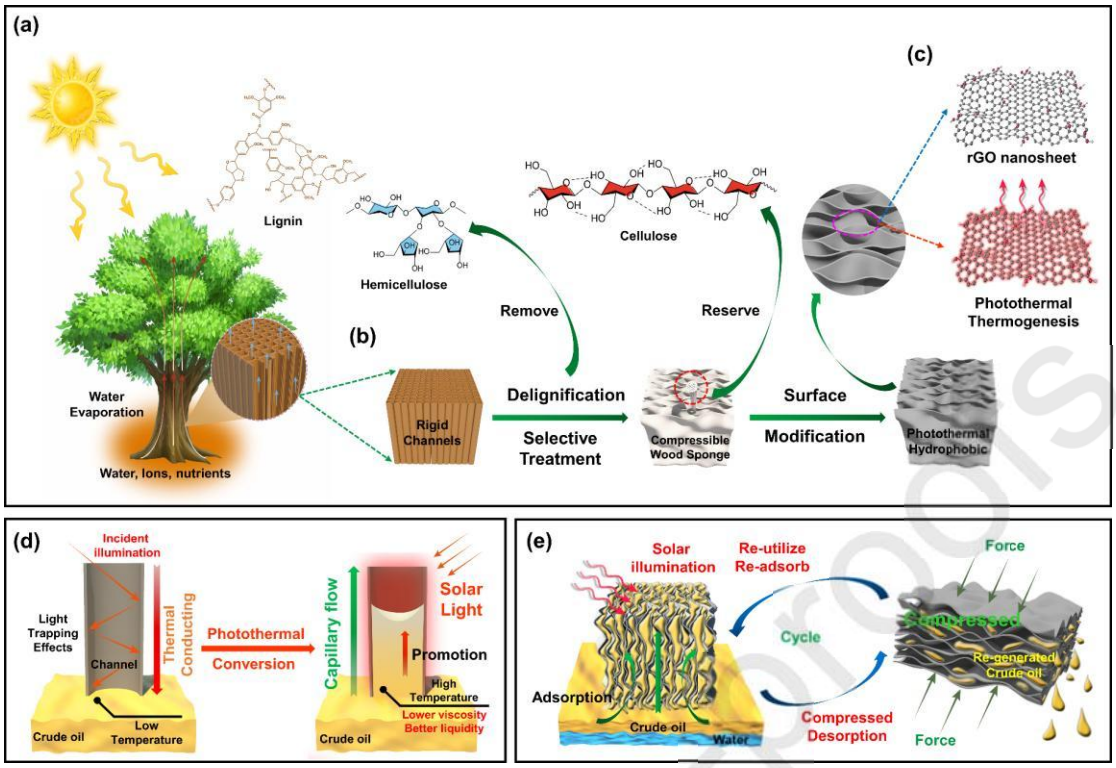

Figure 1. (a) Graphical illustration of naturally grown tree and the solar-motivated evaporation process. (b) Schematic illustration of the fabrication of OTS-rGO-WS from NW through WS. (c) Illustration of photothermal effects of in-situ reduced graphene oxide coating over OTS-rGO-WS. (d) Light-trapping effects in the channels of OTS-rGO-WS and solar-motivated capillary flow for promotion of crude oil through the channels. (e) Adsorption process of crude oil under solar illumination and the regeneration via mechanical compression.

A lamellar-stacked structure of WS after removal of lignin and hemicellulose (**Figure 2a**) was essential for compressibility in contrast to the rigid structure of PW and DW (**Figure S1a, 1b)**. The compressible lamellar-stacked structure was maintained even after subsequent surface decorations with GO (**Figure S1c**), rGO (**Figure S1d)**, and OTS **(Figure 2b)**. FT-IR (**Figure 2c and Table S1)** spectra showed changes in chemical compositions of the material surfaces after each

treatment. The XRD (**Figure S2**) patterns showed the changes in cellulose, wherein after selective removal of lignin and hemicellulose, the cellulose became more crystalline. Moreover, there were characteristic oxygen-containing functional groups, such as hydroxyl groups and ether bonds, between adjacent hexatomic rings in cellulose chains. Further investigations on the channel structure revealed that the porous structure of WS (**Figure S3**) was more suitable for adsorption. Although the adsorption ability of wood sponge decreased slightly after coating with GO and OTS decoration, due to blockage of their pores. The functionalities endowed OTS-rGO-WS suitable for solar-induced crude oil adsorption.

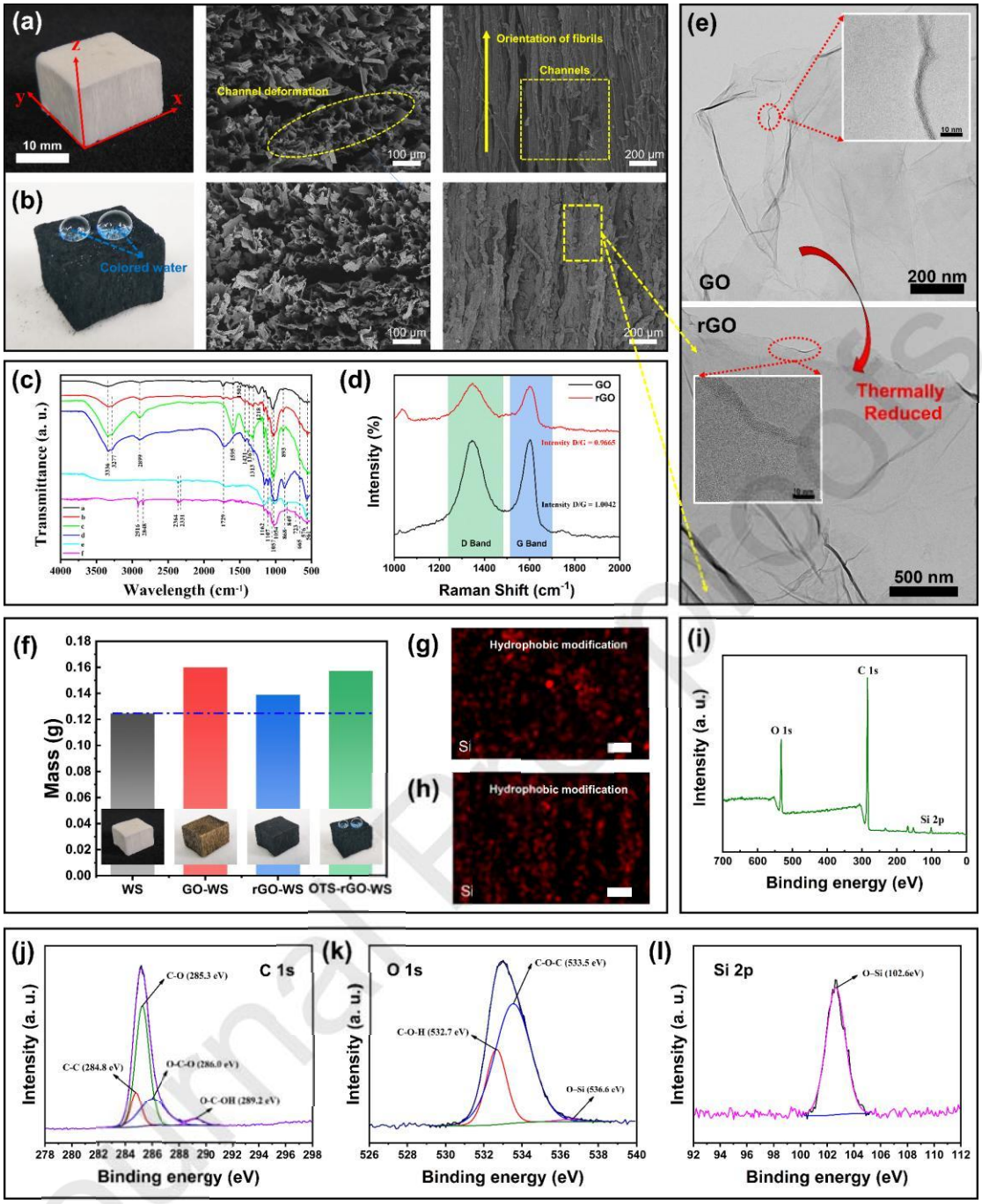

Figure 2. (a, b) Digital photos and SEM images of the cross and longitudinal sections of wood sponge and OTS-rGO-WS, respectively. The scale bar in Figure (a) was applied equally to Figure (b). (c) The FT-IR spectra of (a) PW, (b) DW, (c) WS, (d) GO-WS, (e) rGO-WS, and (f) OTS-rGO-WS. (d) Raman spectra of GO and rGO reduced at 100 °C for 6 h (Excitation wavelength at 532 nm). (e) TEM images of the coating layer above channel wall of OTS-rGO-WS. The coating was fabricated via

GO and thermally reduced GO (rGO), the inset HRTEM images illustrated the refined structures of GO and rGO. (f) The mass changes during fabrication process from WS through GO-WS, rGO-WS to OTS-rGO-WS. (g, h) EDX mapping of Si on OTS-rGO-WS along its cross and longitudinal sections. The scale bar represented a length of 100 μm. (i) XPS survey spectrum of OTS-rGO-WS. (j) C 1s spectrum of OTS-rGO-WS. (k) O 1s spectrum of OTS-rGO-WS. (l) Si 2p spectrum of OTS-rGO-WS.

Raman spectra (**Figure 2d**) demonstrated the efficient reduction of GO to rGO at 100 °C, as indicated by a lower intensity ratio of D band against G band for rGO in removal of defects after the thermal reduction. HRTEM images of GO and rGO (**Figure 2e**) also illustrated the characteristic lattice structure for offering solar-trapping sites during the solar-thermal thermogenesis process. Moreover, XPS spectra of GO-WS and rGO-WS (**Figure S4d-4i**) also indicated the removal of defects-related to oxygen-containing carboxyl and carbonyl functional groups, etc. Notably, GO-WS showed surface composition similar to WS (**Figure S4a-4c**), indicating that GO decoration did not affect the original property of WS. **Figure 2f** shows that 11% of graphene coating (referred to WS) and 13% OTS coating (referred to rGO-WS) were achieved for OTS-rGO-WS, implying that surface modification required little GO.

Hydrophobicity for selective adsorption of oil-phase was achieved, by formation a Si-O bonding on the surface, by immersion of rGO-WS in OTS-hexane solution. Elemental mapping of the cross and longitudinal sections of OTS-rGO-WS (**Figure**

2g, 2h) demonstrated a uniform Si-O bonding layer, which was formed through dehydration and condensation between hydroxyl groups on the surface of the sample. **Table S2** indicated a reduction in O content of OTS-rGO-WS, confirming the dehydrative condensation. XPS spectra (**Figure 2i-2l)** of OTS-rGO-WS verified the presence of Si element in Si-O bonding as a hydrophobic layer. The increased C ratio suggested that dehydrative condensation could also reduce the defects and enhance photothermal conversion. Therefore, the hydrophobic layer was successfully fabricated in OTS-rGO-WS.

3.2 Evaluation of oil adsorption

OTS-rGO-WS exhibited both hydrophobic and oleophilic properties, favorable for selective adsorption of oil-phase and viscous crude oil at high temperature. The adsorption of crude oil could be completed within 1s at 80 °C (**Figure 3a**) and no water wetting occurred (**Figure 3b**). The adsorption of crude oil could not occur at ambient temperature (**Figure 3c**), due to its high-viscosity and low-liquidity. Its resistance to water wetting would be similar to that at high temperature (**Figure 3b, 3d**).

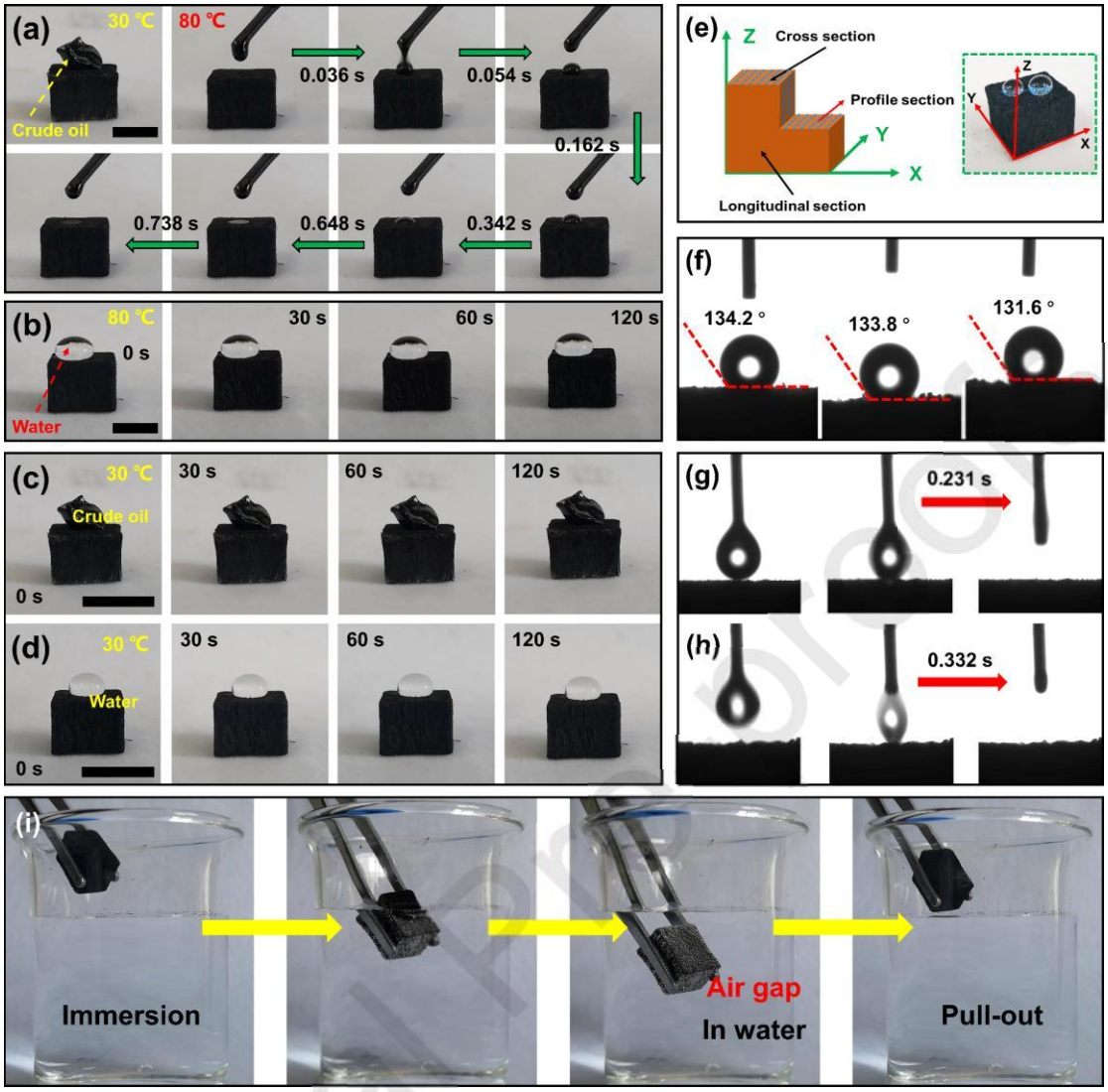

Figure 3. (a) Wetting behavior of crude oil on the surface of OTS-rGO-WS at 30 and 80 °C. (b) Wetting behavior of water at 80 °C on the surface of OTS-rGO-WS. The scale bar in Figure (a) and (b) represent a length of 10 mm. (c) Wetting behavior of crude oil on the surface of OTS-rGO-WS at 30 °C. (d) Wetting behavior of water on the surface of OTS-rGO-WS at 30 °C. The scale bar exhibits a length of 15 mm. (e) Illustration of cross, longitudinal, and profile sections of OTS-rGO-WS, the channel distributions over different sections are illustrated by dashed lines. (f) Seawater contact angle above cross, longitudinal, and profile sections of OTS-rGO-WS. (g, h) Oil (n-hexane) contact angles on OTS-rGO-WS at cross section and longitudinal

section, respectively. (i) OTS-rGO-WS in and out of water and the air gap formed between water and surface of OTS-rGO-WS.

The water contact angles (**Figure 3e)** of OTS-rGO-WS surface were 134.2 °, 133.8 °, and 131.6 ° for the cross, longitudinal, and profile sections (**Figure 3f)**, respectively, revealing uniform hydrophobic and oleophilic properties of the surfaces. Notably, the materials did not exhibit super-hydrophobicity, with water contact angle over 150 °. However, this study actually tried to promote the hydrophobicity by increasing OTS loading content from 1%, 3% to 5% volume ratio, though the contact angle could exceed 150 °, the increasing OTS content formed more and more Si-O bonding on the surface of rGO-WS, which blocks the graphene oxide layer for efficient photothermal thermogenesis (**Figure S5**). To better balance and guarantee sufficient photothermal conversion, in this study, 1% volume ratio OTS was used to fabricate the hydrophobic layer.

For common light oil (n-hexane), OTS-rGO-WS presented a wetting process at the cross and longitudinal sections in 0.231 s and 0.332 s, respectively (**Figure 3g, 3h**). In addition, both passive adsorption and active collection of common oil-phase pollutants could be achieved (**Figure S6**). The maximum adsorption capacities in mass ratios of methylbenzene, xylene, and n-hexane (light oil) and dichloromethane, trichloromethane, and tetrachloromethane (heavy oil) were 5.82, 6.32, 4.58, 9.81, 9.35, and 9.64 g/g, respectively (**Figure S7**). Compared with some artificial materials, the as-prepared materials of this study actually did not exhibit favorable adsorption ability. The reason was the insufficient development of inherent porous structure from natural

wood. However, the compressible property and scale-up accessibility through industrial production could overcome this drawback. Moreover, it can simultaneously solve the problems of crude oil adsorption due to its inherent high-viscosity and clean-up the spillage using more environmental-friendly materials.

Furthermore, it was observed that an air gap was formed on the surface of OTS-rGO-WS in water (**Figure 3i**) due to the hydrophobicity and lipophilicity. This could help trapping adsorbed light energy and reduce the thermal transfer in the longitudinal direction. Since oil spills also occur in the inland river region, the wettability with freshwater, having different density and surface tension, should also be measured. **Figure S8** demonstrated that the contact angle of water phase at the cross section increased to 136.1 ° from 134.2 °, while the contact angle at longitudinal and profile sections did not change remarkably, and remained 134.2 ° and 132.0 °, respectively. These results indicated that the OTS-rGO-WS also has adsorption selectivity in freshwater, like river or lake environment.

Normally, crude oil has high viscosity at room temperature. However, the viscosity decreases remarkably above 60 °C (**Figure 4a**). Thus, solar-thermal thermogenesis of OTS-rGO-WS can raise the temperature for crude oil adsorption. **Figure 4b** shows that OTS-rGO-WS had much higher light absorption than PW and WA. It also showed high thermal conductivity along the **Z** direction and relatively low conductivity along the **X** direction (**Figure 4c**), making more efficient heat transfer from its surface to the oil underneath and reducing thermal diffusion. **Figure 4d** shows temperature variations of OTS-rGO-WS under 1 sun illumination.

OTS-rGO-WS exhibited a fast temperature rise to 80 °C within 100 s. This fast temperature change could thus induce the decrease in crude oil viscosity for adsorption.

A graphical illustration of solar assisted adsorption of crude oil is presented in **Figure 4e**. In this work, a wood sample of 10 mm thickness was allowed to float in a tank containing a 2 mm oil layer and 6 mm water under illumination of 1 sun power (0.1 W/cm^2). The adsorption process of crude oil could be divided into three stages with temperature changes (**Figure 4f**). Firstly, the surface temperature of OTS-rGO-WS increased significantly, since the thermal energy was not yet transferred to the crude oil. Secondly, a fraction of the thermal energy reached the crude oil level and increased its temperature, thereby reducing the viscosity of the crude oil. The relatively cooler crude oil underneath the adsorbent was adsorbed due to capillarity force and the surface temperature of OTS-rGO-WS decreased from its peak value. Finally, the OTS-rGO-WS was saturated with adsorbed crude oil and the temperature of the adsorbed crude oil continued to increase to a constant level under solar illumination. Notably, these adsorption stages reflected well the process of surface temperature changes and the largest mass ratio for adsorbed crude oil reached up to 7.28 g for OTS-rGO-WS per unit mass (**Figure S7**).

In addition to the passive adsorption of crude oil under solar illumination, OTS-rGO-WS could be also used in pumping-assisted separation under 1 sun illumination. Here, a continuous solar-assisted separation system was designed and employed to efficiently collect crude oil (**Figure S9**). A bulk piece of OTS-rGO-WS

with dimensions of 15×15×10 mm^3 was connected to a vacuum pump that operated at -0.2 MPa, through a suction flask as the collector, to extract the floating crude oil over water. A thick layer of crude oil was placed over seawater in a 250 mL beaker. Then, the OTS-rGO-WS was moved to the upper surface of crude oil phase under solar illumination. With the development of photothermal thermogenesis and subsequently induced lower viscosity of crude oil, the oil was collected through vacuum suction into the collector. The extraction process gradually progressed with decrease in viscosity of crude oil, and ca. 50 mL of crude oil for was collected after 900 s. Most of the crude oil could be extracted on illumination for 1200 s. This process illustrated the potential of OTS-rGO-WS to provide a more efficient cleanup strategy of crude oil.

The variation of surface temperature in other related areas (bare crude oil floating over water and floating crude oil approaching the OTS-rGO-WS) was also carefully investigated. For crude oil, the temperature could be increased to ca. 55 °C, whereas the temperature was 50 ºC for crude oil floating over water due to absorption of heat loss by water (**Figure 4g**). Notably, when OTS-rGO-WS floated on crude oil, the temperature of the crude oil surface could reach up to 80 °C within a short time (**Figure 4h**). The temperature gradient thus spontaneously forced the thermal energy to flow from a hotter region to a cooler region through OTS-rGO-WS. These facts demonstrated the role of OTS-rGO-WS in heat transfer. Otherwise, solar illumination of crude oil floating over water could not generate thermal energy sufficient to lower the viscosity of oil. Thus, OTS-rGO-WS as a medium of energy transmission could

promote the temperature rise of the contacted crude oil for faster adsorption. The leaching of oil from OTS-rGO-WS to water was investigated under 1 sun illumination. After a period of 2 h of illumination and 2 h of no light, no crude oil leakage was observed, suggesting the favorable retention of oil by OTS-rGO-WS (**Figure 4i** and **4j)**.

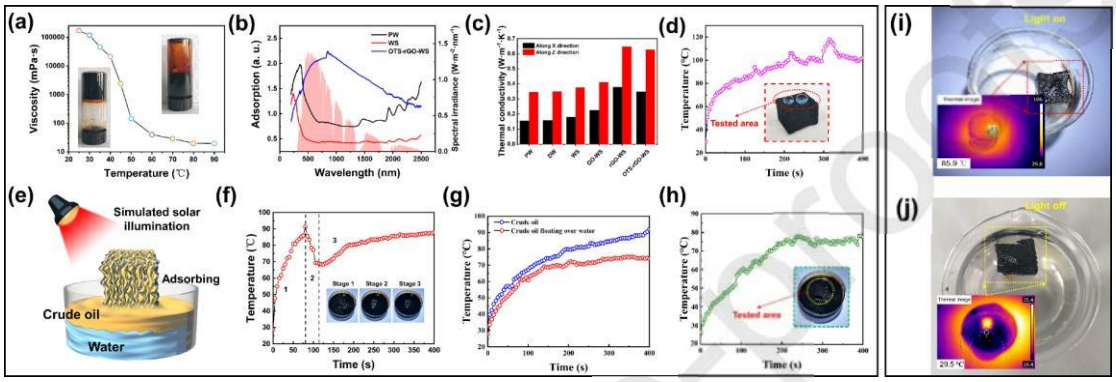

Figure 4. (a) Viscosity of crude oil as a function of temperature. (b) UV-Vis light-absorption spectra for PW, WS, and OTS-rGO-WS. (c) Thermal conductivities for PW, DW, WS, GO-WS, rGO-WS, and OTS-rGO-WS along X and Z directions as illustrated in Figure 2a. (d) Temperature changes on surface of OTS-rGO-WS when exposed to illumination. (e) Graphical illustration of the simulated solar illumination assisted crude oil adsorption. (f) The variation of surface temperature of OTS-rGO-WS floating above the crude oil in water under illumination. The inset photos corresponded to the three stages marked in the curve. (g) Temperature changes for surface of crude oil and surface of crude oil floating over water under illumination. (h) Temperature changes for surface of the crude oil approaching the OTS-rGO-WS absorbent in crude oil under illumination. (i, j) No obvious oil leakage from OTS-rGO-WS at high (85.9 °C) and ambient (29.5 °C) temperatures.

3.3 Numerical modeling of solar assisted adsorption of crude oil

For more understanding of the solar-assisted adsorption process of crude oil, a numerical model from computational fluid dynamics (CFD) was developed (**Figure S10)**. Further information about the modeling analysis is provided in Section 3 of Supplementary Information.

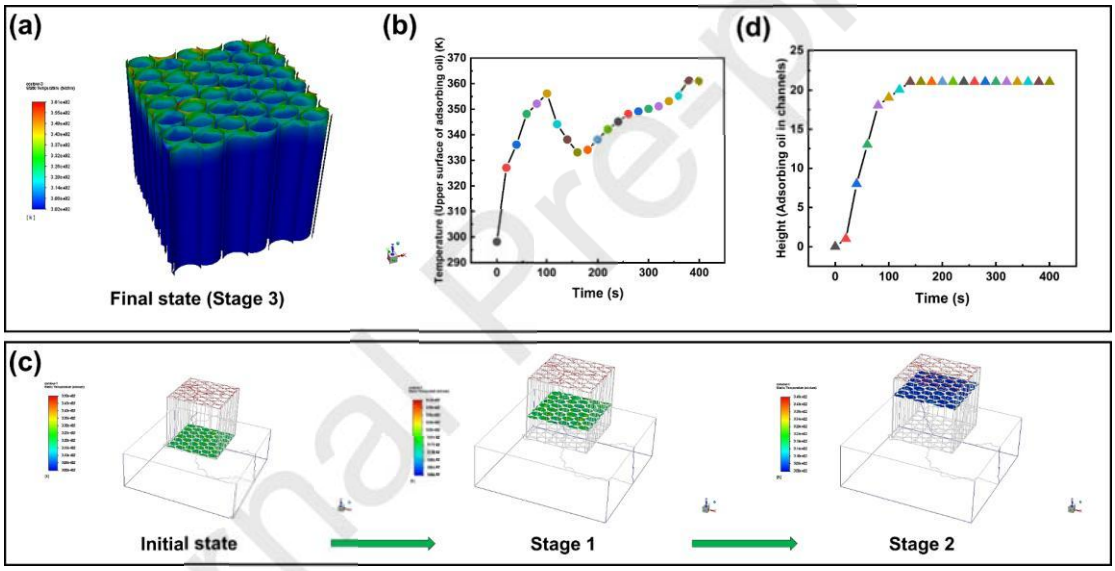

Figure 5. (a) Steady temperature distribution on the upper surface of OTS-rGO-WS with crude oil adsorbed in the channels. (b) Temperature change curve as function of time for crude oil at air-crude oil interface. (c) Simulated stages corresponding to the aforementioned adsorption stages in Figure 4f. (d) The rising speed curve as a function of time for adsorbed crude oil flowing in channels.

Figure 5a showed the final transient temperature distribution on the upper surface of OTS-rGO-WS and **Figure 5b** illustrated the temperature changes at the

air-crude oil interface upon illumination for extended time, which exhibited favorable fitting with the actual measured results. It is believed that, before saturation of the crude oil in channels, a hierarchical temperature gradient always existed from the upper surface of OTS-rGO-WS to air-crude oil interface. The temperature gradient thus resulted in efficient thermal diffusion to the cooler crude oil phase and reduced its viscosity. **Figure 5c** displayed the temperature profiles of the three stages and the results were consistent with the actual measured results. Thus, the temperature variation on the upper surface of OTS-rGO-WS according to the simulations could very well reflect the actual adsorption process. Moreover, these simulations also verified the process of photothermal induced adsorption.

Induced by solar illumination, the viscosity of crude oil in channels decreased and the oil was adsorbed into the channels via capillary-force. Due to the low-viscosity of crude oil and the restrained flow channels, the oil flow could be regarded as a laminar flow. Moreover, the temperature gradient of crude oil adsorbed in the channels was less, and its flow rate in the channels tended to be steady as **Figure 5d** illustrates. Though the heated crude oil had lower viscosity, it should be regarded as a viscous fluid. However, because of the restrained flow in channels, the shearing behavior of adsorbed crude oil in the channels did not show the characteristic features of a viscous fluid. Moreover, the shearing rate tended to level off with increase in time. Promoted by the photothermal conversion and the subsequent capillary-force assisted adsorption, the relatively low-viscosity crude oil was adsorbed into OTS-rGO-WS until it reached saturation. Considering the size of adsorbent

channels and the time interval to attain adsorption saturation, the laminar flow assumption and simulation should be consistent with the reality. Benefiting from the laminar flow, no obvious heat energy loss occurred in the channels (in contrast, turbulence caused a loss in kinetic energy due to random flow). Increased thermogenesis could be conducted directionally along the channels to promote the overall photothermally induced adsorption.

3.4 Hydrophobicity stability and resistance to several surfactants

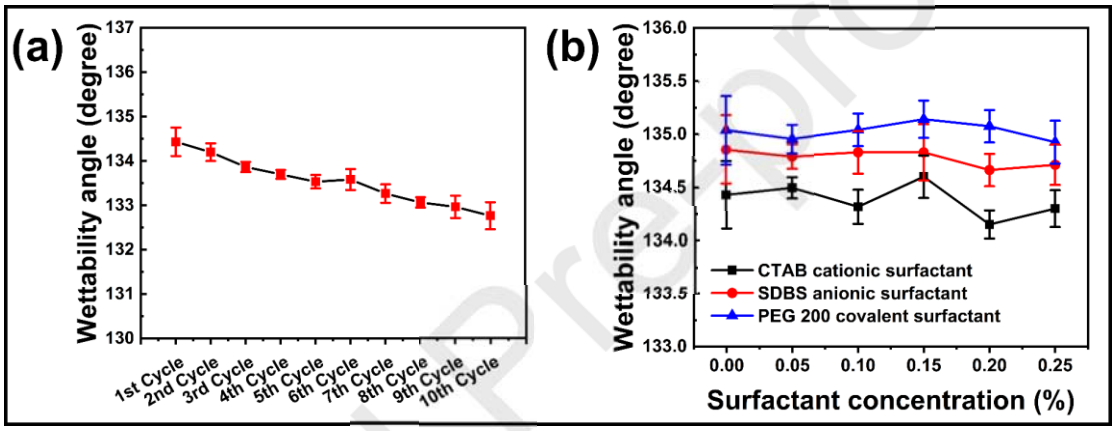

Figure 6. (a) Variations in wettability angle of seawater at the cross section of OTS-rGO-WS through 10 cycles of crude oil adsorption and recovery. (b) Variations in wettability angle of seawater at the cross section of OTS-rGO-WS with different types of surfactants at different concentrations.

Long-term performance stability is essential for practical applications, to demonstrate the hydrophobic stability of materials during their usage. Water wettability measurements of materials through 10 cycles of crude oil adsorption and regeneration were conducted. As shown in **Figure 6a**, the contact angle decreased from an initial 134.2 ° to 132.8 ° through 10 cycles. This slight deterioration demonstrated the favorable stability of the materials during usage. The stability could

be the result of strong bonding between the functional components, including both OTS and rGO with wood sponge matrix. This could be determined by the mutual interactions between oxygen-containing functional groups.

Another problem requiring further consideration is the effect of impurity in oil phase. As the exploitation depth of crude oil increases, some surfactants are usually added into the oil well for increasing the output. The so-called second oil recovery method normally uses some amount of water with surfactants to replace the deep crude oil, resulting in a mixture of water, surfactants, and crude oil. Herein, in this section, the influence of different surfactants on wettability behavior was also investigated. As shown in **Figure 6b**, for all three types of surfactants including CTAB as cationic surfactant, SDBS as anionic surfactant, and PEG 200 as covalent surfactants, the wettability angles did not change remarkably compared to the initial value. These results demonstrated the water resistance of materials in presence of surfactants to some extent and complied better with the real situations.

3.5 Recovery of adsorbed crude oil and numerical modelling

The recovery of adsorbed crude oil normally requires the use of chemical additives and expensive facilities [26, 27]. In contrast, compression and squeezing of sponge-like OTS-rGO-WS allows for simple and economic recovery of the adsorbed crude oil for cyclic uses. **Figure 7a** showed an adsorption-regeneration-adsorption cycle at 60 ºC. Unlike DW, which was not fully recovered after compression (**Figure S11**), OTS-rGO-WS exhibited anisotropically compressible properties and suffered much less stress under the same strain (**Figure 7b**). Notably, the anisotropically

compressible structure of OTS-rGO-WS (**Figure 7d, 7e**) was similar to WS (**Figure S12**), implying that the surface decoration did not affect the structure. The anisotropically compressible properties of OTS-rGO-WS endowed it with excellent mechanical performance, though longitudinal section could not bear too much compressing strain (**Figure 7f**). OTS-rGO-WS exhibited a favorable recovery response at 20-40-60 % strain deformation (**Figure 7g**). Moreover, OTS-rGO-WS possessed excellent cycling compression stability (**Figure 7h**). After 50 and 100 cycles of compression, little reduction in mechanical response properties was observed. A 10-cycle test of adsorption-regeneration-adsorption on OTS-rGO-WS for adsorption of crude oil showed negligible mass change after each cycle (**Figure 7c**), which demonstrated the great cycling stability of the material.

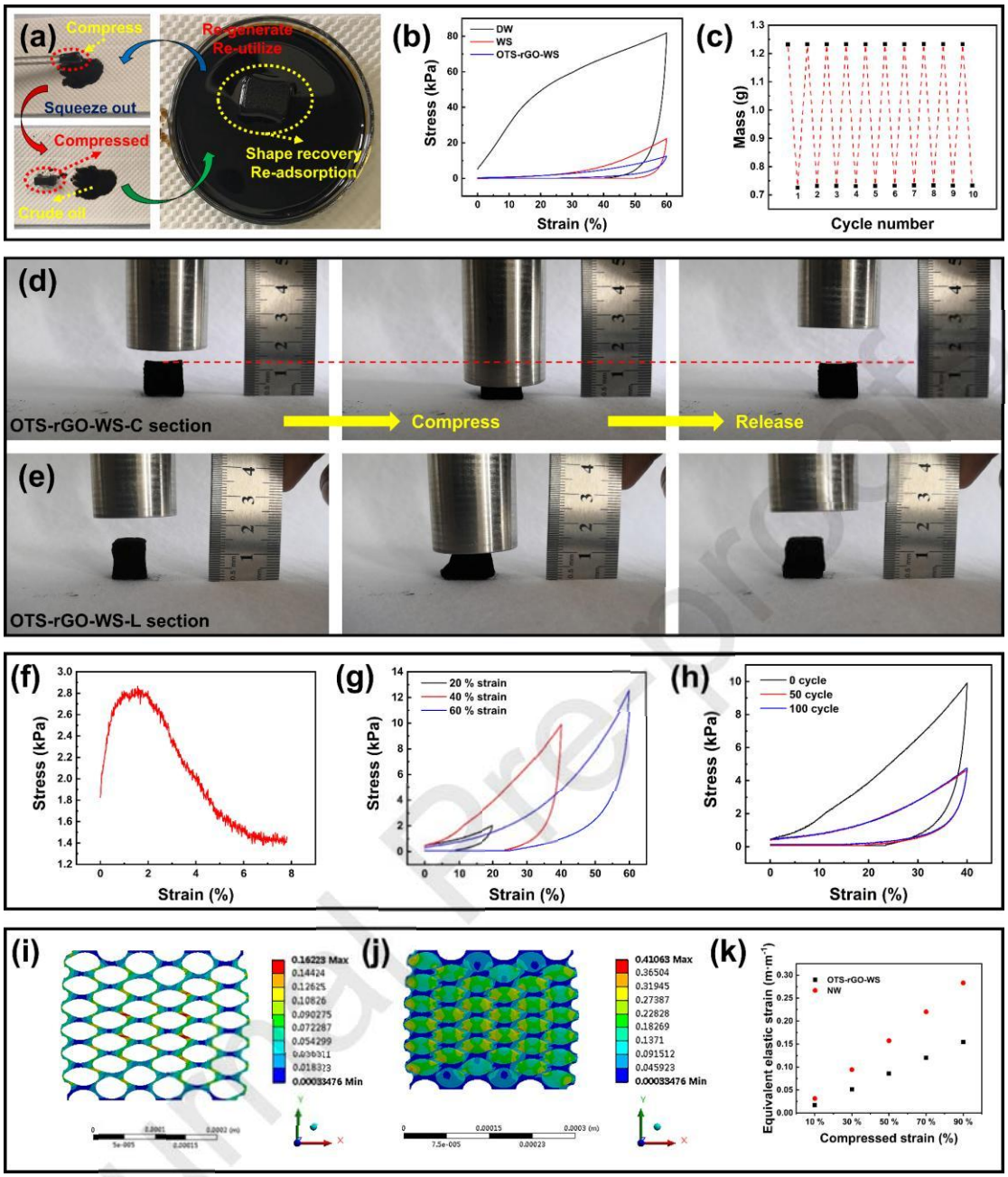

Figure 7. (a) Illustration of adsorption and desorption processes of crude oil via mechanical compression and re-utilization of OTS-rGO-WS. (b) Stress-strain curves of DW, WS, and OTS-rGO-WS under compression at maximum strain of 60 %. (c) Variations in mass of OTS-rGO-WS after 10 cycles of adsorption and desorption at 60 °C. (d) Process showing compressing vertical to the cross-section of OTS-rGO-WS. (e) Process showing deformation along the cellulose-alignment

direction, displaying its anisotropic mechanical properties. (f) Stress-strain curves of OTS-rGO-WS compressed along the cellulose-alignment direction showing its anisotropic mechanical properties. (g) Stress-strain curves of OTS-rGO-WS under compression with hierarchical maximum strains of 20 %, 40 %, and 60 %. (h) Stress-strain curves of OTS-rGO-WS under cyclic compression at the maximum strain of 40 %. (i) Frameworks of OTS-rGO-WS and (j) OTS-rGO-WS with channels filled with low-viscosity crude oil. The normal applied compression corresponded to 30% deformation strain. (k) Simulated results of equivalent elastic strain for OTS-rGO-WS and NW under various compression strains from 10 to 90% with an increment of 20%. Low-viscosity crude oil was then fully filled within the channels under compression.

For comprehensively understanding the structure of OTS-rGO-WS in regeneration of crude oil and the distribution of stress, a numerical model was developed (**Figure S13**). Further information about the calculation method and the modeling analysis is provided in Section 3 of the Supplementary Information.

The modeling of the stress conditions for OTS-rGO-WS with saturated crude oil under compression illustrated that the compressible structure of OTS-rGO-WS exhibited less stress near the structural nodes, compared with the rigid structure (**Figure S14**). The stress distributions under compression of OTS-rGO-WS and rigid PW are presented in **Figure S15-S17**. OTS-rGO-WS showed more resistance to stress and deformation compared to the rigid structure of PW and thus had better mechanical allowance in compression and regeneration of both adsorbed crude oil and

adsorbents (**Figure 7i**).

The compressible structure prevented failure of the adsorbent structure and promoted its cyclic use. Moreover, the stress distribution was more uniform under compression at the structural nodes when low-viscosity crude oil was filled in the channels, which implied that the structural tolerance could be maintained during recovery (**Figure 7j**). With adsorbed crude oil, it was hard to measure the hierarchical compression strain response in OTS-rGO-WS. The different strains were calculated (**Figure 7k** and **S18**). Deformation without structure failure could be achieved below 90% compression strain. A higher acceptable strain value led to more squeezing out of adsorbed crude oil, indicating a great potential for regeneration. These results demonstrated that recovery of crude oil from OTS-rGO-WS could be achieved via a simple compression method.

3.6 Crude oil adsorption from seawater under light illumination

Since most oil spill disasters occur offshore, it is vital to demonstrate the practical applications in seawater environments under solar illumination. Typically, most of the solar power is below 1 sun, and salinity of sea water is 3-4% [53]. In practical use, crude oil was spilled over saline water, and dozens of the OTS-rGO-WS bulks were evenly floated over the crude oil/sea water under artificial sunlight illumination (**Figure S19**). The floating crude oil was completely adsorbed onto the OTS-rGO-WS within 6 h.

Table 1. Comparisons of main parameters and performances between this research and previous results.

Matrix materials	Photothermal components	Maximum temperature	Sun power density	Crude oil adsorption capacity	Regeneration method	Biodegradability	Ref.
Wood sponge	In-situ thermally reduced graphene oxide	88 °C	1 sun	**0.801 g·cm^{-3}**	**Mechanical compression**	**Accessible**	**This research**
Natural wood	Carbonization	61 °C	1 sun	0.694 g·cm^{-3}	None	Partial (As carbonized treatment hindered biodegradation)	[54]
Melamine sponge	Polydopamine (PDA)	79 °C	1.5 sun	1.29 g·cm^{-3}	None	None	[27]
Melamine sponge	Reduced graphene oxide and silver nanoparticles	67 °C	1 sun	1.32 g·cm^{-3}	None	None	[55]
Melamine sponge	Reduced graphene oxide	89 °C	1 sun	1.24 g·cm^{-3}	Mechanical compression	None	[56]
PU sponge	Carbon nanotubes (CNTs)	78 °C	1 sun	3.4×10^{-3} g·cm^{-2}	None	None	[26]
Metal-organic frameworks (MOFs)	Reduced graphene oxide	None	None	None (Adsorption for common heavy and light oil was investigated)	None	None	[13]
Melamine sponge	Reduced graphene oxide	None	None	None (Adsorption for common heavy and light oil was investigated)	None	None	[48]
Melamine sponge	Graphene/carbon black	None	None	None (Adsorption for common heavy and light oil was investigated)	None	None	[15]

Note: The crude oil adsorption capacity of OTS-rGO-WS was derived from the adsorption ratio of 7.28 g/g and the density of 0.16 g / 1.5 cm^3 (0.107 g/cm^3), which resulted in the adsorption capacity by unit mass of 0.801 g/cm^3.

Comparison of the performance of OTS-rGO-WS with previously reported materials is presented in **Table 1** [13, 15, 26, 27, 48, 54-56]. Considering its high-efficiency adsorption, compressible recycling, low fabricating and operational costs, easy scale-up through industrial methods, and practical large-area solar illumination, OTS-rGO-WS is a promising and cost-effective wood-based novel adsorbent for effective mitigation of crude oil spill disasters.

4. Conclusion

A functionalized and compressible wood-based adsorbent was prepared for the adsorption and separation of high-viscous crude oil via in-situ solar-thermal thermogenesis. The fabricated adsorbent exhibited great capacity of oil adsorption (7.28 g/g - 0.801 g/cm^3) and oil collection of 50 mL crude-oil within 20 min. The OTS-rGO-WS showed wide range of applications for light and heavy oil-water separation in passive and active operations and could be operated in sea-water under solar illumination. Numerical modeling calculations were conducted to gain an in-depth understanding of the processes of crude oil adsorption and compressed regeneration. mechanism and related dominant factors were specifically discussed and combined with actual measurement results. Such a material using natural solar illumination represents a promising and functional approach for mitigating crude-oil spillage.

Associated content

Supporting Information: Detailed characterization methods, conditions and equipment model, detailed measurement methods for crude oil adsorbed process, supplementary

data for the components and morphologies of fabricated samples, mechanical and thermal properties measurement for fabricated samples, results for variable controlled experimental groups (Variables were set as GO precursor solution concentration and simulated sun illumination power density), specific illustration for the numerical modelling for dynamic calculation, graphical illustration for the ability of fabricated samples for treating common light oil and heavy oil, the comparison between the main performance of the fabricated samples in this research and other former reported samples (Mainly including temperature rising, crude-oil adsorption capacity, regeneration method and accessibility and biodegradability).

Conflicts of interest

There are no conflicts of interest to declare.

Acknowledgements

This work was supported by the National Natural Science Foundation of China (Grant no. 31770605, Grant no. 31822008) and the Outstanding Youth Foundation of Heilongjiang (Grant no. JC2018006).

Abbreviations

OWSM, Oil/water separation materials; PW, pristine wood; DW, delignified wood; WS, wood sponge with only cellulose framework; GO-WS, graphene oxide (GO) coated WS; rGO-WS, in-situ thermally treated GO-WS; OTS-rGO-WS, octadecyltrichlorosilane (OTS) treated rGO-WS.

References

[1] L. Li, J. Zhang, A. Wang, Removal of Organic Pollutants from Water Using Superwetting Materials, Chemical Record. 18 (2018) 118-136. http://10.1002/tcr.201700029.

[2] X. Wang, J. Yu, G. Sun, B. Ding, Electrospun nanofibrous materials: a versatile medium for effective oil/water separation, Materials Today. 19 (2016) 403-414. http://10.1016/j.mattod.2015.11.010.

[3] Q.B. Thai, D.K. Le, N.H.N. Do, P.K. Le, N. Phan-Thien, C.Y. Wee, H.M. Duong, Advanced aerogels from waste tire fibers for oil spill-cleaning applications, Journal of Environmental Chemical Engineering. 8 (2020) 104016. http://10.1016/j.jece.2020.104016.

[4] J. Ge, L.A. Shi, Y.C. Wang, H.Y. Zhao, H.B. Yao, Y.B. Zhu, Y. Zhang, H.W. Zhu, H.A. Wu, S.H. Yu, Joule-heated graphene-wrapped sponge enables fast clean-up of viscous crude-oil spill, Nature Nanotechnology. 12 (2017) 434-440. http://10.1038/nnano.2017.33.

[5] W. Zhou, Y. Fang, P. Li, L. Yan, X. Fan, Z. Wang, W. Zhang, H. Liu, Ampholytic Chitosan/Alginate Composite Nanofibrous Membranes with Super Anti-Crude Oil-Fouling Behavior and Multifunctional Oil/Water Separation Properties, ACS Sustainable Chemistry & Engineering. 7 (2019) 15463-15470. http://10.1021/acssuschemeng.9b03002.

[6] H. Zhang, Y. Shen, M. Li, G. Zhu, H. Feng, J. Li, Egg Shell Powders-Coated Membrane for Surfactant-Stabilized Crude Oil-in-Water Emulsions Efficient Separation, ACS Sustainable Chemistry & Engineering. 7 (2019) 10880-10887. http://10.1021/acssuschemeng.9b01756.

[7] A. Kumar, G. Sharma, M. Naushad, S. Thakur, SPION/β-cyclodextrin core–shell nanostructures for oil spill remediation and organic pollutant removal from waste water, Chemical Engineering Journal. 280 (2015) 175-187. http://10.1016/j.cej.2015.05.126.

[8] X. He, C. Liang, Q. Liu, Z. Xu, Magnetically responsive Janus nanoparticles synthesized using cellulosic materials for enhanced phase separation in oily wastewaters and water-in-crude oil emulsions, Chemical Engineering Journal. 378 (2019) 122045. http://10.1016/j.cej.2019.122045.

[9] J. Xu, L. Li, J. Wang, Q. Zhang, T. Huang, Efficient oxidation of macro-crude oil in soil using oil-absorbing Fe catalyzing H2O2, Chemical Engineering Journal. 367 (2019) 219-229. http://10.1016/j.cej.2019.02.077.

[10] J. Xu, M. Zhao, R. Wang, J. Du, J. Wang, Q. Zhang, Efficiently dedicated oxidation of long-chain crude oil in the soil by inactive SOM-Fe, Chemical Engineering Journal. 375 (2019) 121913. http://10.1016/j.cej.2019.121913.

[11] J. Jiang, Q. Zhang, X. Zhan, F. Chen, A multifunctional gelatin-based aerogel with superior pollutants adsorption, oil/water separation and photocatalytic properties, Chemical Engineering Journal. 358 (2019) 1539-1551. http://10.1016/j.cej.2018.10.144.

[12] H. Guan, Z. Cheng, X. Wang, Highly Compressible Wood Sponges with a Spring-like Lamellar Structure as Effective and Reusable Oil Absorbents, ACS Nano. 12 (2018) 10365-10373. http://10.1021/acsnano.8b05763.

[13] J. Gu, H. Fan, C. Li, J. Caro, H. Meng, Robust Superhydrophobic/Superoleophilic Wrinkled Microspherical MOF@rGO Composites for Efficient Oil-Water Separation, Angewandte Chemie-International Edition. 58 (2019) 5297-5301. http://10.1002/anie.201814487.

[14] D.D. Nguyen, N.-H. Tai, S.-B. Lee, W.-S. Kuo, Superhydrophobic and superoleophilic properties

of graphene-based sponges fabricated using a facile dip coating method, Energy & Environmental Science. 5 (2012) 7908-7912. http://10.1039/c2ee21848h.

[15] C. Ji, K. Zhang, L. Li, X. Chen, J. Hu, D. Yan, G. Xiao, X. He, High performance graphene-based foam fabricated by a facile approach for oil absorption, Journal of Materials Chemistry A. 5 (2017) 11263-11270. http://10.1039/c7ta02613g.

[16] L. Chen, M. Xia, J. Du, X. Luo, L. Zhang, A. Li, Superhydrophilic and Oleophobic Porous Architectures Based on Basalt Fibers as Oil-Repellent Photothermal Materials for Solar Steam Generation, Chemsuschem. (2019) 493-500. http://10.1002/cssc.201902775.

[17] Z. Zhu, S. Fu, L.A. Lucia, A Fiber-Aligned Thermal-Managed Wood-Based Superhydrophobic Aerogel for Efficient Oil Recovery, ACS Sustainable Chemistry & Engineering. 7 (2019) 16428-16439. http://10.1021/acssuschemeng.9b03544.

[18] S. Lei, M. Zeng, D. Huang, L. Wang, L. Zhang, B. Xi, W. Ma, G. Chen, Z. Cheng, Synergistic High-flux Oil-Saltwater Separation and Membrane Desalination with Carbon Quantum Dots Functionalized Membrane, ACS Sustainable Chemistry & Engineering. 7 (2019) 13708-13716. http://10.1021/acssuschemeng.9b01073.

[19] Q.-Y. Cheng, X.-L. Zhao, Y.-X. Weng, Y.-D. Li, J.-B. Zeng, Fully Sustainable, Nanoparticle-Free, Fluorine-Free, and Robust Superhydrophobic Cotton Fabric Fabricated via an Eco-Friendly Method for Efficient Oil/Water Separation, ACS Sustainable Chemistry & Engineering. 7 (2019) 15696-15705. http://10.1021/acssuschemeng.9b03852.

[20] J. Guo, J.R. Morris, Y. Ihm, C.I. Contescu, N.C. Gallego, G. Duscher, S.J. Pennycook, M.F. Chisholm, Topological Defects: Origin of Nanopores and Enhanced Adsorption Performance in Nanoporous Carbon, Small. 8 (2012) 3283-3288. http://10.1002/smll.201200894.

[21] Z. Zhang, P. Mu, J. He, Z. Zhu, H. Sun, H. Wei, W. Liang, A. Li, Facile and Scalable Fabrication of Surface-Modified Sponge for Efficient Solar Steam Generation, Chemsuschem. 12 (2019) 426-433. http://10.1002/cssc.201802406.

[22] H. Sun, Y. Li, Z. Zhu, P. Mu, F. Wang, W. Liang, C. Ma, A. Li, Photothermal Conversion Material Derived from Used Cigarette Filters for Solar Steam Generation, Chemsuschem. 12 (2019) 4257-4264. http://10.1002/cssc.201901503.

[23] U. Zulfiqar, A.G. Thomas, K. Yearsley, L.W. Bolton, A. Matthews, D.J. Lewis, Renewable Adsorbent for the Separation of Surfactant-Stabilized Oil in Water Emulsions Based on Nanostructured Sawdust, ACS Sustainable Chemistry & Engineering. 7 (2019) 18935-18942. http://10.1021/acssuschemeng.9b04294.

[24] S. Qiu, Y. Li, G. Li, Z. Zhang, Y. Li, T. Wu, Robust Superhydrophobic Sepiolite-Coated Polyurethane Sponge for Highly Efficient and Recyclable Oil Absorption, ACS Sustainable Chemistry & Engineering. 7 (2019) 5560-5567. http://10.1021/acssuschemeng.9b00098.

[25] L. Wu, L. Li, B. Li, J. Zhang, A. Wang, Magnetic, Durable, and Superhydrophobic Polyurethane@Fe_3O_4@SiO_2@Fluoropolymer Sponges for Selective Oil Absorption and Oil/Water Separation, ACS Applied Materials & Interfaces. 7 (2015) 4936-4946. http://10.1021/am5091353.

[26] J. Chang, Y. Shi, M. Wu, R. Li, L. Shi, Y. Jin, W. Qing, C. Tang, P. Wang, Solar-assisted fast cleanup of heavy oil spills using a photothermal sponge, Journal of Materials Chemistry A. 6 (2018) 9192-9199. http://10.1039/c8ta00779a.

[27] C. Zhang, M.-B. Wu, B.-H. Wu, J. Yang, Z.-K. Xu, Solar-driven self-heating sponges for highly efficient crude oil spill remediation, Journal of Materials Chemistry A. 6 (2018) 8880-8885. http://10.1039/c8ta02336k.

[28] C. Ruan, M. Shen, X. Ren, K. Ai, L. Lu, A Versatile and Scalable Approach toward Robust Superhydrophobic Porous Materials with Excellent Absorbency and Flame Retardancy, Scientific Reports. 6 (2016). http://10.1038/srep31233.

[29] C. Yu, C. Yu, L. Cui, Z. Song, X. Zhao, Y. Ma, L. Jiang, Facile Preparation of the Porous PDMS Oil-Absorbent for Oil/Water Separation, Advanced Materials Interfaces. 4 (2017) 1600862. http://10.1002/admi.201600862.

[30] G. Hayase, K. Kanamori, M. Fukuchi, H. Kaji, K. Nakanishi, Facile Synthesis of Marshmallow-like Macroporous Gels Usable under Harsh Conditions for the Separation of Oil and Water, Angewandte Chemie-International Edition. 52 (2013) 1986-1989. http://10.1002/anie.201207969.

[31] H. Bi, X. Xie, K. Yin, Y. Zhou, S. Wan, L. He, F. Xu, F. Banhart, L. Sun, R.S. Ruoff, Spongy Graphene as a Highly Efficient and Recyclable Sorbent for Oils and Organic Solvents, Advanced Functional Materials. 22 (2012) 4421-4425. http://10.1002/adfm.201200888.

[32] X. Gui, J. Wei, K. Wang, A. Cao, H. Zhu, Y. Jia, Q. Shu, D. Wu, Carbon Nanotube Sponges, Advanced Materials. 22 (2010) 617-621. http://10.1002/adma.200902986.

[33] Z. Li, L. Zhong, T. Zhang, F. Qiu, X. Yue, D. Yang, Sustainable, Flexible, and Superhydrophobic Functionalized Cellulose Aerogel for Selective and Versatile Oil/Water Separation, ACS Sustainable Chemistry & Engineering. 7 (2019) 9984-9994. http://10.1021/acssuschemeng.9b01122.

[34] X. Gong, Y. Wang, H. Zeng, M. Betti, L. Chen, Highly Porous, Hydrophobic, and Compressible Cellulose Nanocrystals/Poly(vinyl alcohol) Aerogels as Recyclable Absorbents for Oil-Water Separation, ACS Sustainable Chemistry & Engineering. 7 (2019) 11118-11128. http://10.1021/acssuschemeng.9b00066.

[35] A. Kumar, A. Rana, G. Sharma, S. Sharma, M. Naushad, G.T. Mola, P. Dhiman, F.J. Stadler, Aerogels and metal–organic frameworks for environmental remediation and energy production, Environmental Chemistry Letters. 16 (2018) 797-820. http://10.1007/s10311-018-0723-x.

[36] L.A. Berglund, I. Burgert, Bioinspired Wood Nanotechnology for Functional Materials, Advanced Materials. 30 (2018) 1704285. http://10.1002/adma.201704285.

[37] C. Chen, J. Song, S. Zhu, Y. Li, Y. Kuang, J. Wan, D. Kirsch, L. Xu, Y. Wang, T. Gao, Y. Wang, H. Huang, W. Gan, A. Gong, T. Li, J. Xie, L. Hu, Scalable and Sustainable Approach toward Highly Compressible, Anisotropic, Lamellar Carbon Sponge, Chem. 4 (2018) 544-554. http://10.1016/j.chempr.2017.12.028.

[38] J. Song, C. Chen, C. Wang, Y. Kuang, Y. Li, F. Jiang, Y. Li, E. Hitz, Y. Zhang, B. Liu, A. Gong, H. Bian, J.Y. Zhu, J. Zhang, J. Li, L. Hu, Superflexible Wood, ACS Applied Materials & Interfaces. 9 (2017) 23520-23527. http://10.1021/acsami.7b06529.

[39] A. Jernelov, How to defend against future oil spills, Nature. 466 (2010) 182-183. http://10.1038/466182a.

[40] P. Gong, S. Ji, J. Wang, D. Dai, F. Wang, M. Tian, L. Zhang, F. Guo, Z. Liu, Fluorescence-switchable ultrasmall fluorinated graphene oxide with high near-infrared absorption for controlled and targeted drug delivery, Chemical Engineering Journal. 348 (2018) 438-446. http://10.1016/j.cej.2018.04.193.

[41] R. Li, Z. Li, X. Sun, J. Ji, L. Liu, Z. Gu, G. Wang, Graphene quantum dot-rare earth upconversion nanocages with extremely high efficiency of upconversion luminescence, stability and drug loading towards controlled delivery and cancer theranostics, Chemical Engineering Journal. 382 (2020) 122992. http://10.1016/j.cej.2019.122992.

[42] X. Ye, X. Qin, X. Yan, J. Guo, L. Huang, D. Chen, T. Wu, Q. Shi, S. Tan, X. Cai, pi-pi conjugations improve the long-term antibacterial properties of graphene oxide/quaternary ammonium salt nanocomposites, Chemical Engineering Journal. 304 (2016) 873-881. http://10.1016/j.cej.2016.07.026.

[43] M.-C. Wu, A.R. Deokar, J.-H. Liao, P.-Y. Shih, Y.-C. Ling, Graphene-Based Photothermal Agent for Rapid and Effective Killing of Bacteria, ACS Nano. 7 (2013) 1281-1290. http://10.1021/nn304782d.

[44] H. Ren, M. Tang, B. Guan, K. Wang, J. Yang, F. Wang, M. Wang, J. Shan, Z. Chen, D. Wei, H. Peng, Z. Liu, Hierarchical Graphene Foam for Efficient Omnidirectional Solar-Thermal Energy Conversion, Advanced Materials. 29 (2017) 1702590. http://10.1002/adma.201702590.

[45] L. Zhu, M. Gao, C.K.N. Peh, G.W. Ho, Solar-driven photothermal nanostructured materials designs and prerequisites for evaporation and catalysis applications, Materials Horizons. 5 (2018) 323-343. http://10.1039/c7mh01064h.

[46] V. Nair, M.J. Munoz-Batista, M. Fernandez-Garcia, R. Luque, J.C. Colmenares, Thermo-Photocatalysis: Environmental and Energy Applications, Chemsuschem. 12 (2019) 2098-2116. http://10.1002/cssc.201900175.

[47] X.-H. Li, J.-S. Chen, X. Wang, M.E. Schuster, R. Schloegl, M. Antonietti, A Green Chemistry of Graphene: Photochemical Reduction towards Monolayer Graphene Sheets and the Role of Water Adlayers, Chemsuschem. 5 (2012) 642-646. http://10.1002/cssc.201100467.

[48] W. Liu, H. Jiang, Y. Ru, X. Zhang, J. Qiao, Conductive Graphene-Melamine Sponge Prepared via Microwave Irradiation, ACS Applied Materials & Interfaces. 10 (2018) 24776-24783. http://10.1021/acsami.8b06070.

[49] S. Tang, M. Chen, N. Zheng, Sub-10-nm Pd Nanosheets with Renal Clearance for Efficient Near-Infrared Photothermal Cancer Therapy, Small. 10 (2014) 3139-3144. http://10.1002/smll.201303631.

[50] K. Yang, Y. Li, X. Tan, R. Peng, Z. Liu, Behavior and Toxicity of Graphene and Its Functionalized Derivatives in Biological Systems, Small. 9 (2013) 1492-1503. http://10.1002/smll.201201417.

[51] Y. Zhu, S. Murali, W. Cai, X. Li, J.W. Suk, J.R. Potts, R.S. Ruoff, Graphene and Graphene Oxide: Synthesis, Properties, and Applications, Advanced Materials. 22 (2010) 3906-3924. http://10.1002/adma.201001068.

[52] K.P. Loh, Q. Bao, G. Eda, M. Chhowalla, Graphene oxide as a chemically tunable platform for optical applications, Nature Chemistry. 2 (2010) 1015-1024. http://10.1038/nchem.907.

[53] Z. Liu, B. Wu, B. Zhu, Z. Chen, M. Zhu, X. Liu, Continuously Producing Watersteam and Concentrated Brine from Seawater by Hanging Photothermal Fabrics under Sunlight, Advanced Functional Materials. (2019) 1905485. http://10.1002/adfm.201905485.

[54] Y. Kuang, C. Chen, G. Chen, Y. Pei, G. Pastel, C. Jia, J. Song, R. Mi, B. Yang, S. Das, L. Hu, Bioinspired Solar-Heated Carbon Absorbent for Efficient Cleanup of Highly Viscous Crude Oil, Advanced Functional Materials. 29 (2019) 1900162. http://10.1002/adfm.201900162.

[55] K. Wang, D.Y. Wang, M.Z. Wang, X.X. Dan, L.M. Che, H.H. Xu, H. Zhou, H. Liu, L. Singh, X.E. Wu, Functional photothermal sponges for efficient solar steam generation and accelerated cleaning of viscous crude-oil spill, Solar Energy Materials and Solar Cells. 204 (2020) 110203. http://10.1016/j.solmat.2019.110203.

[56] Y. Wang, L. Zhou, X. Luo, Y. Zhang, J. Sun, X. Ning, Y. Yuan, Solar-heated graphene sponge for high-efficiency clean-up of viscous crude oil spill, Journal of Cleaner Production. 230 (2019) 995-1002.

http://10.1016/j.jclepro.2019.05.178.

There are no conflicts of interest to declare.

Highlights:

- Compressible wood adsorbent with ecological merits for oil-spill collection
- Photothermal effect induced adsorption of high-viscous crude oil pollutants
- Nature derived structure for efficient adsorption and compressible recovery
- Fast photothermal effect as temperature reach up to 88 °C within 100 s under 1 sun
- Potential mechanisms reveal by Computational Fluid Dynamics calculation

Graphical Abstract